PHYSICAL REVIEW B **73**, 024101 (2006)

Solute/defect-mediated pathway for rapid nanoprecipitation in solid solutions: γ surface analysis in fcc Al-Ag

Daniel Finkenstadt[1,3,*] and D. D. Johnson[1,2,3]
[1]*Department of Physics, University of Illinois at Urbana-Champaign, 1110 W. Green Street, Urbana, Illinois 61801, USA*
[2]*Department of Materials Science & Engineering, University of Illinois at Urbana-Champaign, 1304 W. Green Street, Urbana, Illinois 61801, USA*
[3]*Frederick Seitz Materials Research Laboratory, University of Illinois at Urbana-Champaign, 104 S. Goodwin Avenue, Urbana, Illinois 61801, USA*

(Received 13 May 2005; revised manuscript received 30 September 2005; published 3 January 2006)

In face-centered-cubic (fcc) Al, stacking fault energy (SFE) is high at ca. 150 mJ/m^2, inhibiting stacking fault (SF) formation and dislocation motion. Yet Ag-rich hcp precipitates form rapidly in Al-rich fcc Al-Ag, even as the energy difference $\Delta E_{hcp\text{-}fcc}$ between hcp and fcc homogeneous solid solution increases with Ag content. Using electronic density functional theory methods, we calculate the SFE γ_{SF} versus distance of Ag (111) planes from intrinsic (isf), extrinsic (esf) and twin (tsf) SFs. We find that an inhomogeneous distribution of Ag solute segregated in layers adjacent to SFs leads to favorable SFE, a manifestation of the well-known Suzuki effect. We revisit the oft-quoted relation derived at fixed composition of $\gamma_{isf} \simeq \gamma_{esf} \simeq 2\gamma_{tsf} \propto \Delta E_{hcp\text{-}fcc}$, and we show that it holds only for cases that maintain symmetry of the underlying Bravais lattice, e.g., elemental metals and homogeneous solid solutions, and only roughly for certain layered configurations. We show that this defect/solute-mediated, low-energy pathway provides a local mechanism in inhomogeneous solid solution for the rapid hcp precipitation observed in Al-rich fcc Al-Ag.

DOI: 10.1103/PhysRevB.73.024101 PACS number(s): 61.72.Nn

I. INTRODUCTION

Aluminum alloys are highly valued as lightweight materials with high tensile and shear strength, and these mechanical properties may be further improved by precipitation hardening, even at room temperature in dilute alloys. In annealed samples, Guinier and Preston (GP) originally characterized this effect by identifying solute-rich GP zones in Al-Cu (ellipsoidal zones), see Refs. 1 and 2 and in Al-Ag (spherical zones), see Ref. 3, that strengthen alloys by providing obstacles to moving dislocations. Later, Nicholson and Nutting,[4] as confirmed by others,[5–7] identified hexagonal γ-plate precipitates in supersaturated Al–16 at. % Ag alloys. In fact, binary Al-Ag is an ideal prototype for precipitation studies due to its plane-strain transformation and small formation energetics between α-fcc and γ-hcp. The similar fcc lattice spacings[8] of Al (4.05 Å) and Ag (4.09 Å) preclude elastic strain effects, while dissimilar atomic numbers yield high-contrast transmission electron microscopy (TEM) images. Recent TEM results for 4 at. % Ag at 673 K find plates with 40–50 at. % Ag oriented along ⟨111⟩ directions in an otherwise Al-rich matrix[9] (see dark rectangle in Fig. 1). Precipitates grow in minutes as the alloy is quenched from solid solution. Upon subsequent aging at 433 K, spherical GP zones grow throughout the fcc matrix, away from the precipitate which is surrounded by a Ag-depleted zone (see light area around the precipitate in Fig. 1). The observed plate compositions are lower than given by the assessed equilibrium Al-Ag phase diagram, i.e., 59 at. % Ag,[10] and the exact structure of the precipitates remains unknown.

The original Nicholson-Nutting interpretation for rapid γ-plate precipitation was that Ag in *solid solution* reduces the Al alloy stacking fault (SF) energy, allowing local hcp deviations from fcc (111) stacking of crystal planes to occur in the quenched alloy.[4] However, the solid solution does not necessarily have a lower stacking fault energy (SFE) than the solvent (matrix) phase. As discussed by Asta and Johnson[11] and by Zarkevich and Johnson[12] in their calculation of Al-Ag fcc and hcp metastable phase diagrams, respectively, there is an incipient tendency toward segregation in Al-rich bulk Al-Ag solid solutions, as well as Ag-rich hcp ground states. As detailed later, this segregation tendency is evidenced by a highly asymmetric formation energy ΔE_f versus concentration for fcc and hcp solid solutions, shown in Fig. 2(a), in which simple Maxwell construction reveals that Ag-rich regions distributed in a fcc Al matrix form a lower-energy configuration due to the large convexity in ΔE_f versus concentration at large Al content. Such convexity of ΔE_f versus concentration is found in many Al-based systems. Here, using *ab initio* electronic-structure techniques, we quantitatively detail the importance of preferential segregation of solute to a SF defect layer in favoring a hcp phase locally and permitting rapid formation of γ-plate precipitates in fcc Al-Ag. This preferential accumulation of solute atoms at a planar defect, due to a lower ΔE_f of solute atoms at the defect compared to the substitutional solid solution, is a phenomenon known as Suzuki segregation,[13–15] and lowers the SFE, as shown in Fig. 2(b) and discussed in Sec. III.

We note that many researchers have addressed redistribution of solute atoms in alloys near planar defects, using ideas related to the *Gibbs' adsorption isotherm* for interface chemistry. Suzuki[13,14] extended Gibbs' thermodynamic arguments to planar defects in solids, treating the defect as a separate *phase* with different crystal structure and different chemical free energy G^{defect} from the bulk alloy matrix G^{matrix}. For

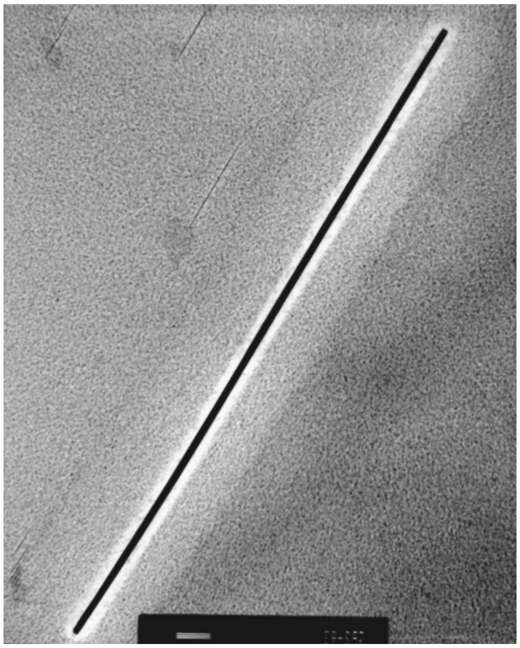

FIG. 1. TEM image of hcp plate precipitate viewed edge on. The broad plates orient along close-packed directions, as described in Ref. 9. Dark regions indicate enhanced Ag concentration, with the plate itself having 40–50 at. % Ag. Surrounding the hcp precipitate is fcc solid solution with 4.2 at. % Ag, except near the plate where Ag is depleted, and the spherical GP zones are obvious. [Reprinted with permission from Acta Mater. **48**, 4090, Copyright (2000) Elsevier (Ref. 9)].

solute fraction X_L in the defect layer and X_0 in the bulk, Suzuki showed that at equilibrium with equal chemical potentials, i.e., $(\partial G^{defect}/\partial X)_{X_L}=(\partial G^{matrix}/\partial X)_{X_0}$, a condition for the interface equilibrium solute fraction[13,14,16] is obtained, namely,

$$\frac{X_L}{1-X_L}=\frac{X_0}{1-X_0}e^{-\Delta G_{seg}/k_BT}, \tag{1}$$

where ΔG_{seg} is the free energy change per solute atom segregated to the planar defect. As described above, Eq. (1) predicts that, for negative ΔG_{seg}, solute redistributes to the defect layer and X_L increases above the bulk value X_0. This result will be useful in guiding the discussion on global versus local solute content.

This paper is organized as follows. In Sec. II, we begin by defining the various types of SF defects and how to determine their energies reliably from electronic-structure methods, especially for homogeneously disordered and segregated layers parallel to the SF. In Sec. III, we calculate the SFE in Al-rich disordered Al-Ag for Ag distributions that are homogeneous and inhomogeneous and find that the SFEs become negative (i.e., SFs have favorable energy) and the ideal shear strength decreases significantly when Ag concentration increases locally at the SF layer. In particular, the lowest-energy configuration is found for Ag planes layered adjacent to a SF forming *locally* the tungsten carbide (WC) structure with alternating Al and Ag (111) planes. For brevity and the mental picture, we will refer to this preferential segregation as *wetting* the defect layer, as Suzuki segregation relates directly to Gibbs' description of wetting at a solid-liquid interface. Generally, then, Suzuki segregation provides a lower free-energy pathway for rapid hcp precipitation, provided there is an inherent tendency for phase segregation in the solid-solution phase, which is a more general mechanism valid not just for fcc Al-Ag. Finally, in contrast to standard arguments relating the SFE to the hcp-fcc energy difference and twin defect energies, at fixed composition, we propose a more general set of relations between minimal energy SF structures and pairs of twin-symmetry-preserving Ag-wetted SF structures.

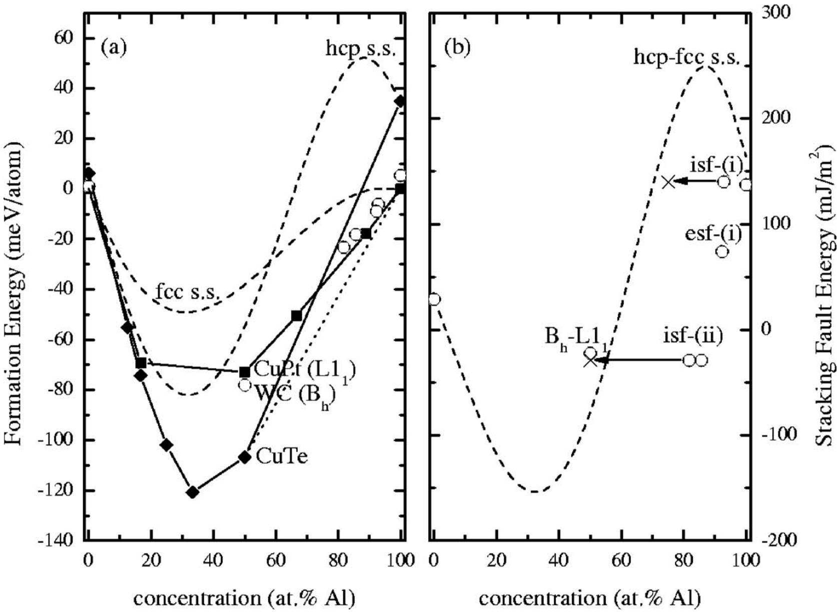

FIG. 2. VASP structural formation energies of (a) fcc and hcp relative to fcc Al and Ag. The fcc-based (square) and hcp-based (diamond) ground states (GSs) are shown along with fcc and hcp solid solution energies (s.s., dashed lines) from Ref. 12. The fcc and hcp GSs intersect near 22 at.% Ag, the maximum solubility of Ag in fcc Al (Ref. 10). At 50 at. % Ag, hcp AlAg is lower than fcc (dotted tieline). Also shown are (b) present results for stacking fault energies at fixed global concentration (open circles) with Ag layers "wetting" the fault in the lowest-energy configuration (see text), and also the hcp-fcc s.s. SFEs estimated using Eq. (2a) (dashed line). These SFEs may be qualitatively represented by a "local" composition within the hcp faulted region, as indicated by arrows ending with crosses (×), which roughly follow the homogeneous s.s. SFE (see text).

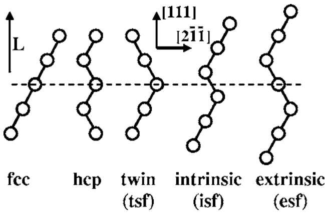

FIG. 3. Close-packed fcc, hcp and faulted fcc, as layered supercells projected onto $(0\bar{1}1)$. Right-climbing (left-climbing) is $ABC(CBA)$ stacking, as in Ref. 19. $L=0$ defines the defect center of mass (dashed line).

II. MODELING STACKING FAULT ENERGIES

In close-packed solids, hexagonal (111) atomic planes stack upon one another like cannonballs. Each successive plane fills the hollows of previous planes, giving traditional "*AB*" ("*ABC*") stacking of hcp (fcc) crystals. However, deviations from perfect stacking order can occur, and the result is a SF defect. SF defects appear along $\langle 111 \rangle$ directions in fcc structures as local ribbons of hcp.[17] Figure 3 illustrates each stacking fault defect, so-called intrinsic (isf) with its missing layer of *A*-stacked atoms, extrinsic (esf) with its extra layer of *B*-stacked atoms, and twin (tsf) with its mirror plane in stacking sequence.[18]

A. SFE relation to hcp-fcc energy difference

In ideal close-packed solids, atoms coordinate tetrahedrally. Considering nearest neighbors, one therefore expects structures in Fig. 3 to be energetically similar. However, locally, hcp order is distinguished from fcc by the bond lengths associated with next-nearest-neighbor planes. The result, as first derived by bond-counting arguments in elemental metals[15,20] *for fixed composition*, is that SF planar defect energies, γ_{isf} and γ_{esf}, are proportional to the hcp-fcc energy difference (per atom) $\Delta E_{hcp\text{-}fcc}$ via the oft-quoted rule of thumb

$$\gamma_{isf} \simeq 2\Delta E_{hcp\text{-}fcc}/A_{111} \tag{2a}$$

$$\simeq \gamma_{esf} \simeq 2\gamma_{tsf}, \tag{2b}$$

where γ_{tsf} is the twin planar defect energy, and A_{111} is the per atom (111) planar area. Equations (2) hold out to fourth-nearest-neighbor relations,[15] but neglect noncentral forces and, thus, fail for the case of *inhomogeneous* solute distribution. We derive in a later section a relationship between chemically ordered γ_{tsf} and similar locally ordered γ_{isf} and γ_{esf}. Our proposed model seeks to explain the calculated ΔE_f and corresponding reduction in SFE for inhomogeneous Ag segregation to the SF, shown in Fig. 2(b). Next we address methods for calculating the SFE accurately.

B. Density functional theory–based cell methods for SFE

To study the structural and formation energetics associated with the SF and its chemically wetted variants, we compare planar-defected systems to their hcp and fcc reference ground states. These comparisons are accomplished via *ab initio* electronic-structure calculations for structural energy difference, for both chemically ordered and disordered systems. These calculations are based on electronic density functional theory (DFT) within the local density approximation (LDA); see, e.g., Ref. 21. We employ two different electronic-structure methods: first, a full-potential, plane-wave method, namely, the Vienna *ab-initio* simulation package (VASP);[22–26] second, the Korringa,[27] Kohn, and Rostoker[28] (KKR) multiple-scattering-based method within the coherent potential approximation[29–31] (CPA) to treat site disorder. As it is not practical to treat compositional disorder using configurational averages, e.g., within VASP calculations, we use the Green's-function-based[32,33] KKR-CPA which allows construction of a DFT for disordered alloys[34,35] and permits accurate calculations of fully (dis)ordered and partially ordered systems as a function of long-range order. The effects of partial order and antisite defects have been shown to be critical for proper comparison of theory to characterization experiments at finite temperature; see, e.g., results in fcc Ni-V,[36] and bcc Fe-Al,[37] as well as defect energies in alloys.[38] All computational details for both methods and convergence may be found in the Appendix.

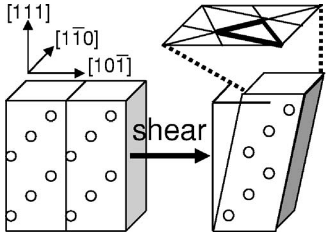

FIG. 4. Schematic of shear from fcc to intrinsic stacking fault structure. Lateral translation of the *c* axis spans the entire footprint of the supercell but can be reduced to an irreducible wedge (highlighted triangle) whose vertices are fcc, isf, and run-on SF configurations. Similarly, isf is sheared into esf by an identical translation on the next adjacent (111) plane.

Several features of Al-Ag simplify calculations immensely. Similar experimentally observed lattice spacings of fcc Al (4.05Å) and Ag (4.09Å) preclude elastic strain effects,[8] so relaxation of cell volume is generally unimportant, at least for qualitative behavior. We calculate using KKR atomic sphere approximation (ASA) and VASP that Al has a cubic lattice constant a_{fcc} of 3.98Å. The KKR-ASA gets that Ag a_{fcc}=3.98 Å, while VASP gets that Ag a_{fcc} =4.02 Å. For the inhomogeneous Al-Ag alloys investigated here, we use a_{fcc}=3.98 Å, giving a common per atom (111) planar area $A_{111}=(\sqrt{3}/4)a_{fcc}^2$=6.86 Å^2. Also there is essentially no *c*-axis distortion for hcp Al, so c/a is ideal, i.e., $\sqrt{8/3} \simeq 1.633$. We note, however, that full ionic relaxation was permitted in each defected cell, while the overall defect cell lattice constants were fixed at multiples of the pure Al translation vector so that no volume relaxation was needed (or, as verified, should be expected).

One method for calculating the SFE uses sheared fcc cells to produce SF structures, e.g., the isf illustrated in Fig. 4. Along the shear path to the isf, there is an *unstable stacking fault* (usf) energy barrier γ_{usf} and a maximum ideal pure shear strength σ_{ideal} associated with the structural transformation, as discussed later. Similar shear on the next adjacent (111) plane yields an esf. By using sheared fcc cells, we calculate σ_{ideal}, γ_{usf}, γ_{isf}, and γ_{esf} for pure Al and for inhomogeneous Al-Ag alloys. For a sheared SF structure with N layers and energy E^{SF}, the planar defect energy is

$$\gamma_{SF} = \frac{E^{SF}(N) - E^{fcc}(N)}{A_{111}}, \tag{3}$$

where E^{fcc} is the *unsheared* reference energy. This sheared-cell method we refer to as *cell method A*.

Another method to calculate the SFE avoids sheared cells by fixing the shape and varying the number of (111) planes. For a fcc structure, cells must be of size $N=3n$, for integer $n>0$. Twin and hcp structures must be of size $N=2n$, and the SF structures must have sizes of $N=3n\pm1$, corresponding to addition or deletion of a layer (see Fig. 3). Comparison between fcc, twin, and hcp is easily done for $N=6n$, but for a SF, an interpolation procedure is necessary,

$$\gamma_{SF} = \frac{E^{SF}(3n\pm1) - \left[\frac{2}{3}E^{fcc}(3n) + \frac{1}{3}E^{fcc}(3n\pm3)\right]}{A_{111}}. \tag{4}$$

From Eq. (4) the reference state is obtained as an interpolation of total energies between two fcc cells with $3n$ and $3n\pm3$ layers but with exactly the same local chemical environment as the SF cell with $3n\pm1$ layers. As the local chemical environment is fixed in the cell, there is little to no effect on the SFE from interpolation due to a Friedel-like oscillation if the cells are large enough ($n>3$). We refer to the interpolation method as *cell method B*. Importantly, cell method B always leads (as it should) to good agreement with the sheared-cell results (see Table I).

For a check on our methods, we compare our results for fcc Al, which has high experimentally assessed[39,40] γ_{SF} of $120-170$ mJ/m^2 that inhibits SF formation and dislocation motion, to earlier results by Wright[41] (plane-wave pseudopotential) and Mishin[42] (full potential linear augmented plane-wave) for γ_{SF} and $\Delta E_{hcp\text{-}fcc}$ (see Table I). We find the γ_{isf} and γ_{esf} are both $130-140$ mJ/m^2 for pure Al, comparable to twice γ_{tsf} of 62 mJ/m^2, in accord with Eq. (2b). Table I lists results and cell methods for pure Al and indicates that, for all methods, mechanical strength and stability against SF formation is high, e.g., compared to the Al-Ag alloy. Notably, previous calculations find $\Delta E_{hcp\text{-}fcc} \sim 38$ meV/atom, giving an estimate from Eq. (2a) of 175 mJ/m^2 for γ_{isf}.

As is clear for smaller unit cells (fewer than 12 layers) we agree with the previous SFE for pure Al, while for 12 or more layers we are converged and are near the experimental value of γ_{isf}. As in previous studies,[42] 5–9 planes are enough to converge the SFE for pure Al to roughly ±10 mJ/m^2, but Ag impurity planes situated directly between the SF and its periodic image require larger cells. This is especially the case for esf using sheared-cell method A due to the decreased separation between planar faults. For reliable convergence in the alloy case, we use 12 layers for sheared structures using the cell method A, and we use six (12,13, and 14) layers for hcp (tsf, esf, and isf) using cell method B.

TABLE I. Al and Al-Ag calculated stacking fault and γ-surface parameters given by *ab initio* methods and experiment (expt.). Structures (i) and (ii) are for one and two Ag-wetting planes, respectively. The hcp-fcc energy difference $\Delta E_{hcp\text{-}fcc}$ (in meV/atom) is reported, along with SF energies (in mJ/m^2, ±5 mJ/m^2) and ideal shear strength σ_{ideal} (in GPa). Within VASP, we used method A via sheared cells with 12 layers and method B via hexagonal cells with 12- (13-,14-)layer tsf (esf, isf) using the interpolated $3n$-layer fcc structure. In parentheses for method A, we show results for a nine-layer sheared cell that are slightly underconverged both for pure Al isf and for esf due to the decreased separation between planar faults in the same nine-layer cell.

	Previous work		Present work					
	Pure Al		Pure Al		Al-Ag (i)		Al-Ag (ii)	
	Expt.	Theory	A	B	A	B	A	B
$\Delta E_{hcp\text{-}fcc}$		38[a]		35				−5.1
γ_{tsf}	75[b]	75[a,c]		62		−3		−29
γ_{isf}	120[d]	165[a],158[e]	133	136	140	140	−21	−29
	165[b]	146[c]	(149)		(139)		(−29)	
γ_{esf}	170[b]	154[a]	140	132	78	74	17	16
			(152)		(79)		(26)	
γ_{usf}		168[c], 175[e]	174		168		58	
σ_{ideal}		2.84[e]	2.72		2.69		1.23	

[a] Plane-wave pseudopotential from Ref. 41.

[b] Experimental results from Ref. 39.

[c] Full potential linear augmented plane wave from Ref. 42.

[d] From Ref. 40, a reinterpretation of experimental results in Ref. 39.

[e] VASP shear calculations from Ref. 43.

III. STACKING FAULT ENERGIES FOR (IN)HOMOGENEOUS SOLID SOLUTIONS

In the past, it is often assumed that the solid-solution, random, substitutional alloy is treated as a homogeneous system, such that arguments leading to Eq. (2) hold and are used to estimate the γ_{SF} from hcp and fcc solid-solution mixing curves. Homogeneous disorder is difficult to address in most computational methods, but we are able to treat it here using the KKR-ASA method within the coherent potential approximation (CPA). Calculated KKR-CPA-ASA mixing energies, relative to pure Al and Ag fcc, are shown for hcp and fcc Al-Ag in Fig. 5(a). The convex curvatures of hcp and fcc ΔE_f in the Al-rich end indicate an incipient tendency toward precipitation, which is the origin for the observed miscibility gap.[11] The dotted line in Fig. 5(a) shows the expected thermodynamic ($T=0$ K) equilibrium state, namely, dilute fcc solid solution plus Ag-rich hcp precipitates, in accord with the experimentally observed hcp plates shown in Fig. 1.

From the hcp-fcc energy difference shown in Fig. 5(b), we see that $\Delta E_{hcp\text{-}fcc}$ can increase with Ag content. Therefore if we employ the naive bond-counting result for γ_{SF}, the SFE should increase proportionally to $\Delta E_{hcp\text{-}fcc}$ and SF formation becomes unfavorable. The erroneous conclusion from calculations that the observed SFE should be unaffected or *increased* by addition of solute is one made many times over in the literature.[6,44–46] As an example, Ref. 46 reports mixing energies and SFE for three Al alloys and obtains quantitative

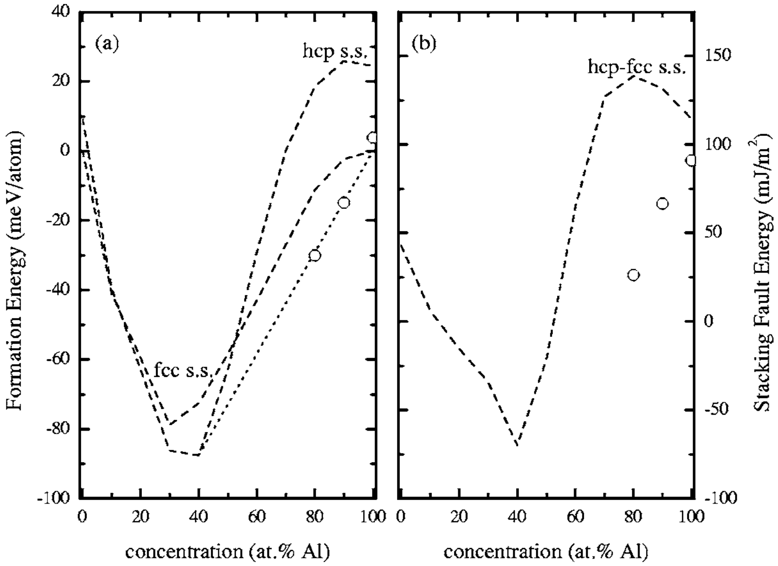

FIG. 5. KKR-CPA-ASA solid-solution mixing energies (s.s., dashed lines) of (a) fcc and hcp relative to fcc Al and Ag. Also shown are (b) extrinsic stacking fault energies (esf, open circles) with zero, one, and two Ag layers wetting the esf within a ten-layer cell. The hcp-fcc s.s. curve gives estimates of stacking fault energy using Eq. (2a), valid for homogeneously disordered Al-Ag. Lattice constant was fixed to that of fcc Al, i.e., a_{fcc}=3.98 Å.

agreement between calculated SFE and predicted SFE obtained by Eq. (2a) using hcp and fcc solid-solution mixing curves—but these predicted SFEs are not relevant to what should be observed in the actual alloy system. That is, the conclusions of Ref. 46 suggest an *increase* of SFE with a small addition of Ag to pure Al. This mistaken application of the simple relation in Eq. (2a) to predict the SFE contradicts expectations from Suzuki segregation[13] given in Eq. (1) requiring that solute should be either (1) energetically favored at the SF and lower SFE, or (2) energetically unfavored at the SF and hence diffuse away from the SF and not increase SFE above that of the matrix phase.[15] Furthermore, the observed Ag-rich hcp precipitates found in Al-Ag suggest there *must* be a mechanism by which the fcc→hcp structural phase transformation is rapid.[9]

To address Suzuki segregation in Al-Ag, we determine the γ_{isf} and γ_{esf} as the location of a single Ag layer is varied versus distance from the fault. As shown clearly in Fig. 6, γ_{SF} is significantly lowered by having the Ag layer adjacent to the fault. So lower-energy pathways are available for reduction of free energy. Furthermore, Fig. 6 also reports the effect on γ_{SF} when a second Ag layer is introduced on the opposite side of the SF, with the minimum also directly adjacent to the fault. Clearly then Ag preferentially *wets* the SF. These results confirm that the Suzuki effect is operative. We note that we could further introduce a third Ag on either side to study its most favored position, or, using the KKR-CPA, permit a solid solution of Ag in the remaining Al layers along with the two Ag layers straddling the SF (which shifts the composition). Both of these calculations would be interesting and lead to even better understanding of the effects of distributions of solute, but we have not yet looked at these in favor of understanding the effects on a shear surface.

In Fig. 6, as Ag planes are moved away from the SF, there are oscillations in SFE, roughly approaching the bulk value. This oscillation in the SFE is reminiscent of tight-binding-based calculations by Redfield and Zangwill[47] that found the chemical potential for a SF is a Friedel-like, damped, oscil-

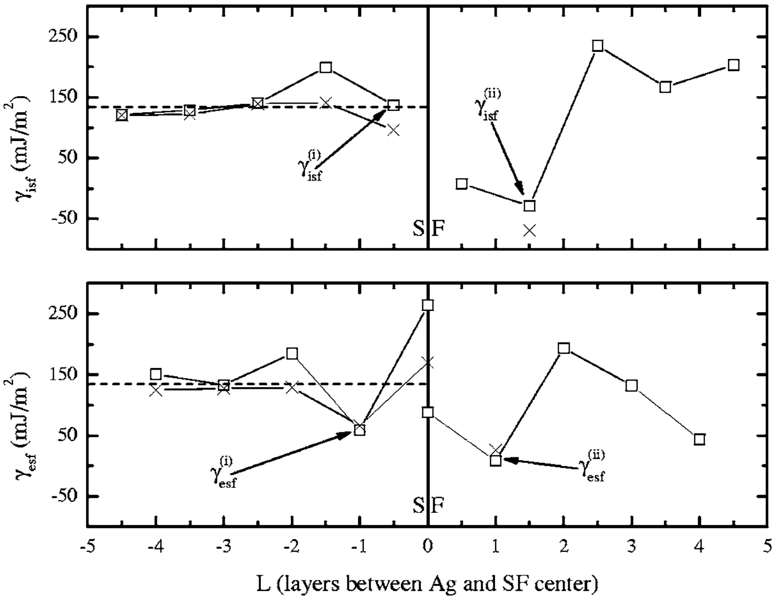

FIG. 6. KKR-ASA (×) and VASP (squares) γ_{isf} and γ_{esf} for Ag planes inserted L (111) planes away from SF defect in fcc Al. L is defined in Fig. 3. One Ag plane is brought in from the left. The minimum-energy structures for one Ag plane are labeled $\gamma_{isf}^{(i)}$ and $\gamma_{esf}^{(i)}$. The first Ag planes are held fixed at $\gamma_{isf}^{(i)}$ and $\gamma_{esf}^{(i)}$, and a second Ag plane is brought in from the right. The minimum-energy structures for two Ag planes are labeled $\gamma_{isf}^{(ii)}$ and $\gamma_{esf}^{(ii)}$. The labels (i) and (ii) correspond to isf and esf with one and two Ag-wetting planes, respectively. The dashed lines indicate bulk Al SFEs from VASP. All calculations are done using cell method B for 11-layer isf and 10-layer esf cells with estimated error of ±10 mJ/m^2.

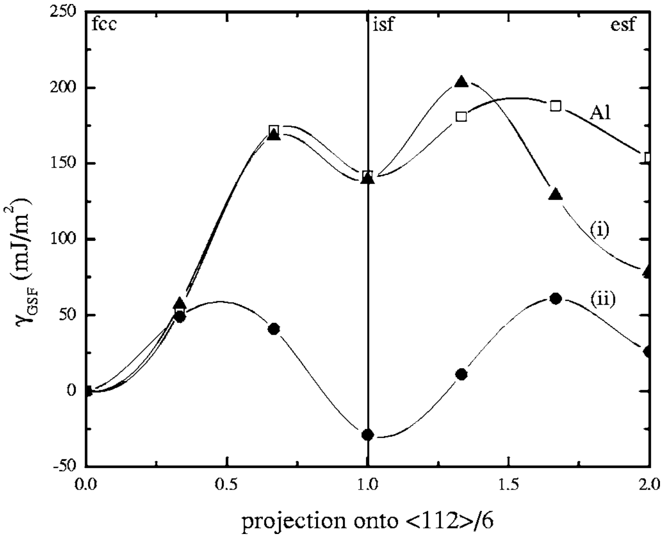

FIG. 7. Traces of the VASP generalized stacking fault energy (or γ) surface along $\langle 112\rangle$ directions for Al and Ag-wetted faults in Al-Ag. Shear in $\langle 112\rangle$ directions connects fcc to isf and, on the next adjacent slip plane, connect isf to esf. Squares are pure Al. (i) Filled triangles are SF wetted by one Ag plane. (ii) Filled circles are SF wetted by two Ag planes. All calculations are done using cell method A for nine-layer cells with estimated error of ±10 mJ/m^2.

latory function of the SF distance from a bimetallic interface. For two Ag layers straddling $L=0$ symmetrically, the γ_{esf} drops to a tenth of its bulk value (dashed line in Fig. 6) while γ_{isf} becomes negative. At fixed global composition, proportionality between γ_{isf} and γ_{esf} in Eq. (2) is thus clearly broken for the case of Ag wetting, and also the calculated SFE is drastically lower than predicted from the solid-solution $\Delta E_{hcp\text{-}fcc}$.

The assumptions leading to Eq. (2) were based entirely on consideration of elemental solids or a *homogeneous* distribution of solute for the necessary bond-counting arguments to work. Therefore, with solute redistribution into layers due to Suzuki segregation, the bond-counting arguments need to account for the inhomogeneous chemical environment around a Ag-wetted SF. Below we show that it is possible to replace Eq. (2) with expressions relating one- and two-layer Ag-wetted γ_{isf} and γ_{esf} to specific combinations of γ_{tsf}.

A. γ-surface for (un)wetted defects

Important shear mechanical parameters can be calculated using cell method A, e.g., the intermediary structures between stable fcc and metastable isf in Fig. 4. Three important extremal structures, of which two are fcc and metastable SF and the third is "atop" stacking, enclose what is called the generalized stacking fault revealed as a surface contour plot or γ *surface*. Extremals in the γ surface are connected by

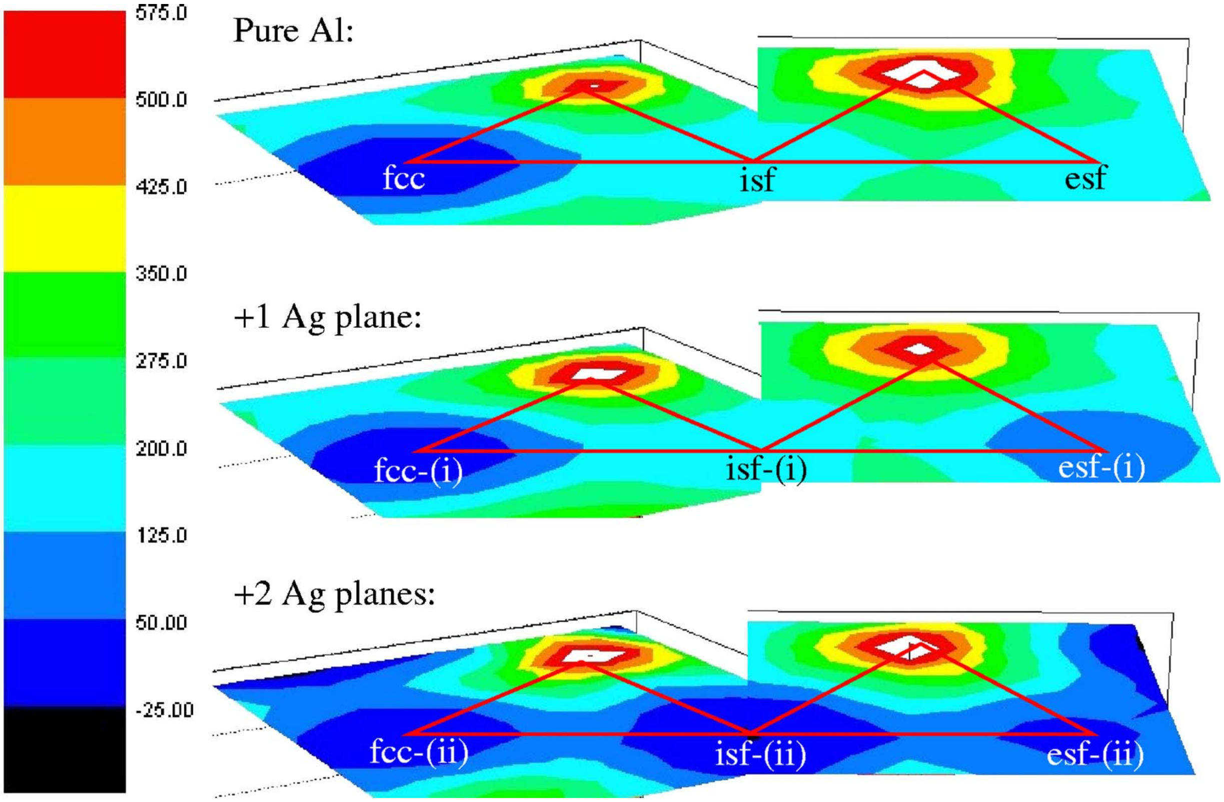

FIG. 8. (Color online) Contour plots of calculated (VASP) Al and Al-Ag γ surfaces, in mJ/m^2. Extrema in the γ surface occur at vertices of the irreducible wedge of shear translations (highlighted triangles, as in Fig. 4). Stable and metastable minima are labeled with structures from Fig. 9. Unstable structures (tops of triangles) are run-on stacking sequences. Triangle sides indicate $\langle 112\rangle/6$ translations, with contours interpolated from a hexagonal array of gridpoints with spacing of $\langle 112\rangle/18$. All calculations are done using cell method A for nine layers.

$\langle 112\rangle/6$ Burgers partial translations. The ideal pure shear strength σ_{ideal} is simply the maximum gradient of $\gamma_{GSF}(\mathbf{f})$, the planar defect energy as a function of shear $\mathbf{f}$. The σ_{ideal} and energy barrier γ_{usf} are calculated by shearing along the fcc→isf portion of the γ surface. Results for pure Al are illustrated in Figs. 7 and 8 and show that mechanical strength and stability against SF formation is very high in pure Al. Importantly, we find that high shear must be applied, and a high energy barrier must be overcome, to achieve local fcc→hcp structural transformation.

The SFE is related to the σ_{ideal} of a material, i.e., the minimum shear required to permanently deform the structure. Recent theoretical modeling based on electronic-structure calculations find that the breaking and formation of directional bonds in Al are correlated with high SFE and determine the $\{111\}\langle 11\bar{2}\rangle$ σ_{ideal} in fcc Al.[43,48] Here, we extend the findings of Ogata, Li, and Yip[43] to Al-Ag alloys. Using cell method A for a nine-layer supercell, we add planes of Ag in the vicinity of a SF to see how it affects structural energies and the γ surface. By varying the position of Ag planes, γ_{SF} is greatly reduced by SF-solute interactions and the shear barriers are seen to be quite low (see Figs. 7 and 8 and Table I). These results establish that SF-solute interactions are *attractive*, i.e., solute wetting reduces the SFE via Suzuki segregation of solute to defect.

The symmetry of γ_{isf} and γ_{esf} are broken for alloys, as in Fig. 9. γ_{esf} is halved by adding Ag, and isf becomes stable (i.e. negative γ_{isf}) over fcc when a SF is decorated in a local WC structure. Essentially the minimum-energy configuration for a dilute alloy is a phase-segregated strip of hcp AlAg within fcc Al matrix. The isf-(ii) is thus structurally and compositionally consistent with a γ plate, as shown in Fig. 1. The energy barrier to formation of isf-(ii) is also lowered to 58 mJ/m^2; see Fig. 7 at $\langle 112\rangle/12$. For low γ_{SF}, SF formation is thus not inhibited if, e.g., thermal or applied strain forces are present, and this provides a mechanism for rapid precipitation.

B. Improved SF model

The energetics of layered configurations of Ag-wetted SF defects are understood by comparing twin defects of given Ag "decoration" to corresponding SF structures of identical decoration. This is accomplished by considering isf and esf as two closely spaced twins. By adding energies of local twins we find that estimates in Eq. (2) generalize to

$$\gamma^{\mathrm{Al}}_{isf} = \gamma^{\mathrm{Al}}_{esf} = 2\gamma^{\mathrm{Al}}_{tsf},$$

$$\gamma^{(i)}_{esf} = \gamma^{(i)}_{tsf} + \gamma^{\mathrm{Al}}_{tsf},$$

$$\gamma^{(ii)}_{isf} = \gamma^{(i)}_{tsf} + \gamma^{(ii)}_{tsf},$$

$$\gamma^{(ii)}_{esf} = 2\gamma^{(i)}_{tsf}. \qquad (5)$$

Here (i) and (ii) refer to special one- and two-layer Ag wetted structures, as in Fig. 9.

The twin energies in Eqs. (5) may be extended to include nonsymmetric twin energies, but only minimum energy structures are considered here. Nonsymmetric tsf structures are useful to predict, e.g., barrier heights in Fig. 6. Comparisons of low-energy SF energies, as well as their alloy formation energies, are given in Table II, where Eqs. (5) are seen to accurately estimate the SFE. Table II also verifies that, with increasing Ag content, local fcc→hcp structural formation becomes increasingly favorable, especially for the case where two-layer Ag wetting planes decorate local hcp.

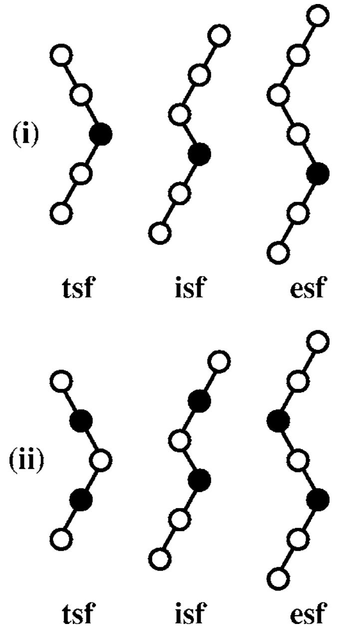

FIG. 9. Close-packed alloy stacking fault structures. Open (closed) circles represent atomic (111) planes of Al (Ag), as in Fig. 3. Labels (i) and (ii) indicate one and two Ag planes, respectively.

Why does dually wetted tsf-(ii) have such a dramatic effect on SFE? To answer this, Fig. 10 shows the change in charge density upon generating a tsf between two Ag layers. Examining the charge density profile and density of states, we find that that by going from fcc structure with Ag two layers apart to the tsf structure with Ag again two layers apart, the bands of Al-Ag are lowered slightly in the vicinity of the Fermi level due to second-nearest-neighbor bonding between stacked Ag planes occupying B sites. The $d(z^2)$ orbitals of each Ag now bond more strongly across the sym-

TABLE II. VASP structurally relaxed planar defect energies γ_{SF} (in mJ/m^2, ±5 mJ/m^2) from Table I and formation energies ΔE_f (in meV/atom, open circles in Fig. 2) relative to fcc Al and Ag. Symbols (i) and (ii) refer to structures in Fig. 9. The WC (B_h) structure relative to CuPt ($L1_1$) is also listed for comparison.

At. % Al	Structure	Eqs. (5)	VASP γ_{SF}	ΔE_f
100	isf	$2\gamma^{\mathrm{Al}}_{tsf}=124$	136	+4.2
93	isf-(i)		140	−6.1
92	esf-(i)	$\gamma^{\mathrm{Al}}_{tsf}+\gamma^{(i)}_{tsf}=59$	74	−8.9
86	isf-(ii)	$\gamma^{(i)}_{tsf}+\gamma^{(ii)}_{tsf}=-32$	−29	−18.1
82	isf-(ii)	$\gamma^{(i)}_{tsf}+\gamma^{(ii)}_{tsf}=-32$	−29	−23.2
50	WC (B_h)	$\gamma^{(i)}_{tsf}+\gamma^{(ii)}_{tsf}=-32$	−22	−78.0

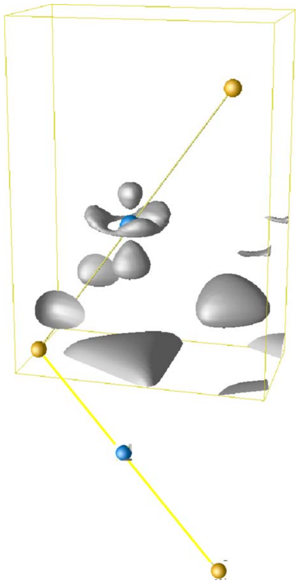

FIG. 10. (Color online) Calculated isosurface of charge density *increase* due to creation of a twin stacking fault interface with two planes of Ag atoms symmetrically straddling the twin interface in Al fcc matrix. Only charge density on one side of the tsf is shown, the other side being mirror symmetric. The isosurface is chosen for an increase of one electron per atomic volume.

metric twin interface, and atoms are pulled inward toward the twin when relaxations are included.

IV. DISCUSSION

As discussed by Asta and Johnson[11] and by Zarkevich and Johnson[12] in their calculation of the metastable Al-Ag fcc and hcp phase diagrams, respectively, there is an incipient tendency for precipitation, evidenced by the highly asymmetric solid solution ΔE_f for fcc and hcp, as shown in Fig. 2(a). Standard Maxwell construction from ΔE_f for fcc and hcp given in Fig. 2(a) reveals that a new ground-state hcp structure[12] at 50 at. % Ag precipitated and distributed throughout a pure fcc Al matrix is the correct thermodynamic state. Importantly, however, at 50 at. % Ag a hcp AlAg tungsten carbide structure is lower in energy than all fcc structures, labeled "WC" in Fig. 2(a). Local similarity of AlAg layered hcp to dual-wetted isf structure, i.e., $\gamma_{isf}^{(ii)}$ in Fig. 9, allows large reduction in γ_{SF} and rapid precipitation, both consistent with the incipient tendency for precipitation due to asymmetric solid solution ΔE_f. Growth of precipitates is modeled in this picture as a series of ordering steps.

(1) Solute segregation to lower γ_{SF} promotes Ag-wetted SF formation, creating planes of increased Ag concentration.

(2) γ_{SF} is high where Ag is depleted, inhibiting further hcp formation, which leads to high-aspect-ratio precipitates.

(3) Local equilibrium is thus established between growth of Ag-wetted SF defects and the Ag-depleted zone.

Thus, as shown by the energetics in Fig. 2, local heterogeneity of the Ag solute allows a large reduction in SFE and thereby facilitates production of SF defects, especially as the local concentration surpasses ~22 at. % Ag, the point at which the chemically ordered hcp phase becomes favorable over fcc. Solute attraction to the SF, e.g., Ag wetting, provides a local pathway to precipitation that mimics the actual thermodynamic state, hcp AlAg+fcc Al, when more favorable single and double Ag planes segregate around the SF. Reduction of γ_{SF} allows growth of precipitates by partial dislocation motion, and, in this picture, growth is confined to platelike geometry by the large γ_{SF} in surrounding Ag-depleted regions, i.e., that of pure Al (ca. 140 mJ/m^2). Of course, segregation requires vacancy-assisted migration of Ag for kinetics, which leads to a Ag depletion layer around the precipitate, exactly as observed in Fig. 1.

A. Global versus local solute composition

At this point it is worth noting that our results and formulas do not require distinguishing global (i.e., bulk) versus local concentration of solute. In fact, this is important in that "local" solute concentration is, at best, subjectively defined. That is, from Eq. (1) and our SFE calculations, the solute content of Ag X_L within the layer near the defect increases above the bulk (or global) X_0. We have already clearly shown that the SFE decreases at fixed global (bulk) solute content, driven by a local increase in solute within layers around the SF. Thus, to define a local solute composition one must choose a number of layers N surrounding a SF defect giving $c_{local} \approx \Sigma_i^N X_i/N$. Although subjective, by choosing sensibly N to be only the number of hcp-like layers, we find the results in Fig. 2(b), where the SFEs at global composition are given as open circles and the same values at the effective "local" composition are given by the crosses. For example, at global content of 82% Ag, $\gamma_{isf}=-29$ mJ/m^2, and has a local composition of 50%. Hence, locally the structure resembles two unit cells of ordered WC at 50% Ag embedded in a fcc Al matrix. Note, also, from Fig. 2(a) that WC and CuPt structures both are more stable than the hcp solid solution. To get an approximate SFE from these ordered phases, the fcc reference state must have the same local chemical layering as the hcp ordered cell. From Eq. (2), we use $\Delta E_{hcp\text{-}fcc} \approx (E^{\mathrm{WC}} - E^{\mathrm{CuPt}})/6 = -5.1$ meV/atom, as in Table I where the energies are for six-layer hexagonal (111) cells, to obtain an estimate of $\gamma_{isf\text{-WC}}=-22$ mJ/m^2. The planar area is that of fully relaxed CuPt. Clearly the directly calculated γ_{isf} for global Ag content of 82% is consistent with the value found here from an ordered alloy approximately at 50% Ag, as shown in Fig. 2(b). In general, the comparison may not be exact because the $\Delta E^{\text{hcp-fcc}}$ using these ordered phases include an infinite array of SF defects, rather than a single defect layer. The final, interesting point when viewing the directly calculated SFE for fixed bulk composition with this definition of local composition is that γ_{isf} with layers of Ag decorating the SF roughly follows the SFE for the homogeneous solid solution [see Fig. 2(b) where two SFEs at different compositions are shown]. Basically, there is a rough agreement because the solute particle number locally is the same, and the solid solution at this effective local composition reflects an average over all local chemical arrangements including the layered structures near 50% Ag; however, the solid solution includes structures that do not reflect the (111) layered configuration, such as the CuTe structure in Fig. 2(a).

B. Nucleation and growth model

In order to predict growth and real times for comparison to experiment there must be more than the present defect/solute-mediated model; there must be a nucleation and growth model for the precipitate. Elsewhere we show that such a model can be developed based upon the present results. However, in addition to this Suzuki segregation thermodynamic driving force, the kinetics requires interface energies that control growth. Hence, interfaces between the preciptate and the fcc matrix phase, i.e., (0001)/(111) and $\langle 1\bar{1}00\rangle/\langle 112\rangle$, must be determined accurately. Planar fault energies calculated here may be used in an edge growth model, generalized to a hcp structure, to predict the time dependence of the aspect ratio,[49] as will be presented elsewhere.

V. CONCLUSIONS

Using first-principles electronic-structure methods, we found that the SF energy γ_{SF}, while high in pure fcc Al, is significantly reduced and made energetically favorable in Al-rich Al-Ag alloys by the wetting of Ag (111) planes adjacent to the fault at positions that preserve local twinlike symmetry. This effect is most dramatic, reducing γ_{SF} to $-29\ \mathrm{mJ/m^2}$ (from $+136\ \mathrm{mJ/m^2}$ in Al), when alternating planes of Al-Ag-Al-Ag decorate an isf, similar to the hcp tungsten carbide structure. The reason for this chemical ordering is due to favorable Ag-Ag bonding interactions across local *twinlike* interfaces that occur in SF defects. Calculating the shear-energy (or γ) surface of Al-Ag, we find the energy barrier to form a local tungsten carbide SF structure from fcc is $\sim 58\ \mathrm{mJ/m^2}$, and the ideal pure shear strength of the alloy is reduced from 2.72 GPa in pure Al to 1.23 GPa in a dual-Ag-wetted intrinsic SF structure. The low energy of solute-SF wetting provides a defect-mediated, local mechanism that explains the observed rapid hcp high-aspect-ratio precipitate growth in Al-Ag and surrounding Ag-depleted regions, and can be considered a general manifestation of Suzuki segregation. Our results show that the oft-quoted rule that $\gamma_{isf} \approx \gamma_{esf} \propto \Delta E_{hcp\text{-}fcc}$ is not correct in general for alloys. We derived more general relations to predict SF energy based on twin SF and hcp structures having locally similar chemical ordering. Finally, the present mechanism (and equations developed) is quite general and only requires an alloy formation energy that has convex and concave behavior, leading to an incipient phase segregation.

ACKNOWLEDGMENTS

We acknowledge discussions with A. V. Smirnov at the beginning of the project on defect cells, as well as KKR development. Funding is by DOE at the Frederick Seitz MRL (Grant No. DEFG02-91ER45439), NSF ITR (Grant No. DMR-03-25939) at the Materials Computation Center, and ITR (Grant No. DMR-0121695) at the Center for Process Simulation and Design.

APPENDIX: COMPUTATIONAL DETAILS

For Brillouin zone integration a Monkhorst-Pack[50] special k-point method is used. We converge k meshes for hexagonal cells composed on fcc (111) planes stacked along $\langle 111\rangle$ directions, with up to $24\times 24\times 24$ k points in the full Brillouin zone used for primitive fcc cells. The k meshes for larger supercells are determined for equal density of points, with up to $24\times 24\times 8$ k points in the full Brillouin zone used for three fcc planes along $\langle 111\rangle$ (three layers/cell) and with $24\times 24\times 3$ k points to achieve similarly dense coverage in the longest supercells (8–15 atoms/cell). Issues of k-mesh convergence and methods are detailed elsewhere,[41] with k-mesh densities, etc., similar to ours.

For computational expediency, the KKR method is implemented within the atomic sphere approximation.[51,52] As the lattice constants of Al and Ag have similar values, we choose radii of the ASA spheres to be equal in the alloy, an approximation found to be reliable across composition using full-potential linearized muffin tin orbital methods.[11] Lattice constants were fixed to that of fcc Al, $a_{fcc}=3.98$ Å, which ignores relaxations for intermediate-composition structures, e.g., $\mathrm{Ag_2Al}$, but this is addressed later by allowing for full relaxations using the pseudopotential method. For the KKR-ASA, we include $s-$, $p-$, $d-$, and f-type orbital symmetries in the basis set and utilize with a Von Barth and Hedin local exchange-correlation potential.[53] Scalar-relativistic effects (Darwin and mass-velocity terms) are included for core and valence wave equations, but spin-orbit effects are ignored in the valence band. Contour integration over energy[34,54] in the relevant valence band range is used to obtain self-consistent charge density. In particular, we use Gauss-Legendre integration with 18 energy points [see, e.g., Ref. 55 for discussion of accuracy and Ref. 56 for discussion of $O(N)$ computational scaling with number of atoms N]. For our prototype system of Al-Ag, issues of convergence in defect cell size, etc., were calculated using KKR-ASA and differ very little from the results for VASP and are not reported.

We use the KKR-CPA to address the effects of disorder due to compositional variation, which is relevant to assessing competing phases in precipitation. While the computationally efficient KKR-ASA-CPA method treats homogeneous and inhomogeneous systems within the same approximations, there are limitations due to the ASA assumption of spherical cell shape that lead to SFEs that are 20–30 % lower than estimated from experiment.[39] Truncation errors may be corrected using full-potential methods with correct cell shape,[41] or alternatively, errors due to the spherical approximation of cell shape may be addressed by Voronoi polyhedral integration.[57] To be more quantitative, we use the VASP pseudopotential plane-wave method for verification of our findings using KKR-CPA-ASA and for calculation of the Al-Ag γ surface that requires full ionic relaxations.

For VASP calculations,[22–26] ultrasoft pseudopotentials suggested by Vanderbilt[58] are supplied by Kresse and Hafner.[59] LDA exchange-correlation energy is from Ceperley and Alder[60] as parametrized by Perdew and Zunger.[61] Energy cutoffs for plane-wave basis sets are converged to 275 eV (200 eV) for Al (Ag) fcc structures. A cutoff of 275 eV is used for alloys. For accurate calculation of strain relaxation in the direction normal to the close-packed plane, VASP energies are reported here with full ionic relaxations converged to minimize forces to less than 50 meV/Å.

*Electronic address: daniel.kris@gmail.com

[1] A. Guinier, Nature (London) **142**, 569 (1938).
[2] G. P. Preston, Nature (London) **142**, 570 (1938).
[3] A. Guinier, J. Phys. Radium **8**, 142 (1942).
[4] R. B. Nicholson and J. Nutting, Acta Metall. **9**, 332 (1961).
[5] J. A. Hren and G. Thomas, Trans. Metall. Soc. AIME **227**, 308 (1963).
[6] M. Ferrante and R. D. Doherty, Acta Metall. **27**, 1603 (1979).
[7] K. E. Rajab and R. D. Doherty, Acta Metall. **37**, 2709 (1989).
[8] N. W. Ashcroft and N. D. Mermin, *Solid State Physics*, 1st ed. (Saunders College Publishing, Fort Worth, 1976).
[9] K. T. Moore and J. M. Howe, Acta Mater. **48**, 4083 (2000), Fig. 6.
[10] A. McAlister, Bull. Alloy Phase Diagrams **8**, 526 (1987).
[11] M. Asta and D. D. Johnson, Comput. Mater. Sci. **8**, 64 (1997).
[12] N. A. Zarkevich and D. D. Johnson, Phys. Rev. B **67**, 064104 (2003).
[13] H. Suzuki, Sci. Rep. Res. Inst. Tohoku Univ. A **4**, 455 (1952).
[14] H. Suzuki, J. Phys. Soc. Jpn. **17**, 322 (1962).
[15] J. P. Hirth and J. Lothe, *Theory of Dislocations* (McGraw-Hill, New York, 1968).
[16] A. Coujou and P. Coulomb, Scr. Metall. **22**, 1841 (1988).
[17] Q. Jin, P. Wang, D. Ding, and D. Wang, Phys. Lett. A **174**, 437 (1993).
[18] F. C. Frank, Philos. Mag. **42**, 809 (1951).
[19] N. M. Rosengaard and H. L. Skriver, Phys. Rev. B **47**, 12865 (1993).
[20] J. W. T. Read, *Dislocations in Crystals* (McGraw-Hill, New York, 1953), Chap. 7, pp. 92–95.
[21] R. M. Dreizler and E. K. U. Gross, *Density Functional Theory*, 1st ed. (Springer-Verlag, New York, 1990).
[22] G. Kresse and J. Hafner, Phys. Rev. B **47**, R558 (1993).
[23] G. Kresse, Ph.D. thesis, Technische Universitat, 1993.
[24] G. Kresse and J. Furthmuller, Comput. Mater. Sci. **6**, 15 (1996).
[25] G. Kresse and J. Furthmuller, Phys. Rev. B **54**, 11169 (1996).
[26] G. Kresse and D. Joubert, Phys. Rev. B **59**, 1758 (1999).
[27] J. Korringa, Physica (Amsterdam) **13**, 392 (1947).
[28] W. Kohn and N. Rostoker, Phys. Rev. **94**, 1111 (1954).
[29] P. Soven, Phys. Rev. **156**, 809 (1967).
[30] D. W. Taylor, Phys. Rev. **156**, 1017 (1967).
[31] J. S. Faulkner and G. M. Stocks, Phys. Rev. B **21**, 3222 (1980).
[32] D. D. Johnson, D. M. Nicholson, F. J. Pinski, B. L. Gyorffy, and G. M. Stocks, Phys. Rev. B **41**, 9701 (1990).
[33] D. D. Johnson and F. J. Pinski, Phys. Rev. B **48**, 11553 (1993).
[34] D. D. Johnson, F. J. Pinski, and G. M. Stocks, Phys. Rev. B **30**, 5508 (1984).
[35] D. D. Johnson, D. M. Nicholson, F. J. Pinski, B. L. Gyorffy, and G. M. Stocks, Phys. Rev. Lett. **56**, 2088 (1986).
[36] D. D. Johnson, A. V. Smirnov, J. B. Staunton, F. J. Pinski, and W. A. Shelton, Phys. Rev. B **62**, R11917 (2000).
[37] A. V. Smirnov, W. A. Shelton, and D. D. Johnson, Phys. Rev. B **71**, 064408 (2005).
[38] J.-B. Liu, D. Johnson, and A. Smirnov, Acta Mater. (to be published).
[39] L. E. Murr, *Interfacial Phenomena in Metals and Alloys* (Addison-Wesley, Reading, MA, 1975).
[40] R. H. Rautioaho, Phys. Status Solidi B **112**, 83 (1982).
[41] A. F. Wright, M. S. Daw, and C. Y. Fong, Philos. Mag. A **66**, 387 (1992).
[42] Y. Mishin, D. Farkas, M. J. Mehl, and D. A. Papaconstantopoulos, Phys. Rev. B **59**, 3393 (1999).
[43] S. Ogata, J. Li, and S. Yip, Science **298**, 807 (2002).
[44] C. Laird and H. I. Aaronson, Acta Metall. **17**, 505 (1969).
[45] R. D. Doherty and K. E. Rajab, Acta Metall. **37**, 2723 (1989).
[46] T. C. Schulthess, P. E. A. Turchi, A. Gonis, and T. G. Nieh, Acta Mater. **46**, 2215 (1998).
[47] A. C. Redfield and A. M. Zangwill, Phys. Rev. B **34**, 1378 (1986).
[48] N. Kioussis, M. Herbranson, E. Collins, and M. E. Eberhart, Phys. Rev. Lett. **88**, 125501 (2002).
[49] D. Finkenstadt, Ph.D. thesis, University of Illinois at Urbana-Champaign, 2005.
[50] H. J. Monkhorst and J. D. Pack, Phys. Rev. B **13**, 5188 (1976).
[51] O. K. Andersen, Phys. Rev. B **12**, 3060 (1975).
[52] *The Electronic Structure of Complex Systems*, edited by P. Phariseau and W. M. Temmerman (Plenum Press, New York, 1984).
[53] U. von Barth and L. Hedin, J. Phys.: Condens. Matter **5**, 1629 (1972).
[54] R. Zeller and J. Deutz and P. H. Dederichs, Solid State Commun. **44**, 993 (1982).
[55] A. V. Smirnov and D. D. Johnson, Phys. Rev. B **64**, 235129 (2001).
[56] A. V. Smirnov and D. D. Johnson, Comput. Phys. Commun. **148**, 74 (2002).
[57] A. V. Smirnov (private communication).
[58] D. Vanderbilt, Phys. Rev. B **41**, R7892 (1990).
[59] G. Kresse and J. Hafner, J. Phys.: Condens. Matter **6**, 8245 (1994).
[60] D. M. Ceperley and B. J. Alder, Phys. Rev. Lett. **45**, 566 (1980).
[61] J. P. Perdew and A. Zunger, Phys. Rev. B **23**, 5048 (1981).